On elastic response of disordered triangular lattice during dynamic loading

Sreten Mastilovic *

Abstract

The present investigation focuses on an observation regarding the initial elastic response of a triangular geometrically and structurally disordered lattice during medium-to-high strain rate loading. Namely: a transition from the short-time modulus of elasticity to the long-time one, which is not accompanied by the corresponding change of the stiffness tensor. It is demonstrated that the difference between the two moduli is, in the case of the homogeneous biaxial test simulations performed herein, a consequence of the geometrical and structural disorder "quenched" within the lattice. The investigation is performed on the triangular lattice with the first-neighbor central interactions under practically identical in-plane conditions over eight decades of strain rate.

Keywords: Lattice, Discrete Models, Modulus of elasticity, Disorder, Short-time response, Long-time response, Plane strain

1 Introduction

The disordered two-dimensional (2D) triangular lattice is used extensively to study damage evolution and fracture of inhomogeneous or multi-phase systems (e.g., [1, 4, 5, 6, 9, 10]). The objective of this study is to elucidate a perplexing change of modulus of elasticity that accompanies dynamic response of said lattice in the medium-to-high strain rate domain [5, 6].

The dynamic simulations of a uniaxial homogeneous tension test presented herein are performed under practically identical in-plane stress/strain conditions, although they span the strain rate range of eight orders of magnitude.

*Faculty of Construction Management, Union University, Cara Dusana 62-64, 11000 Belgrade, Serbia, e-mail:gmvv@eunet.yu

The lattice simulations are performed at twelve different loading rates within the range $[1\,s^{-1},\ 1\cdot10^8\,s^{-1}]$ in such a way that the normal stress in the loading (longitudinal) direction is the only non-zero in-plane stress component. Hence, normal stress and strain components in the longitudinal direction are, for brevity, called stress and strain, unless specified otherwise.

The plot of the stress (divided by the modulus of elasticity of the pristine material) versus the strain is presented in Fig. 1, for three typical strain rates.[1] The curves in Fig. 1 correspond intentionally to the largest level of geometrical
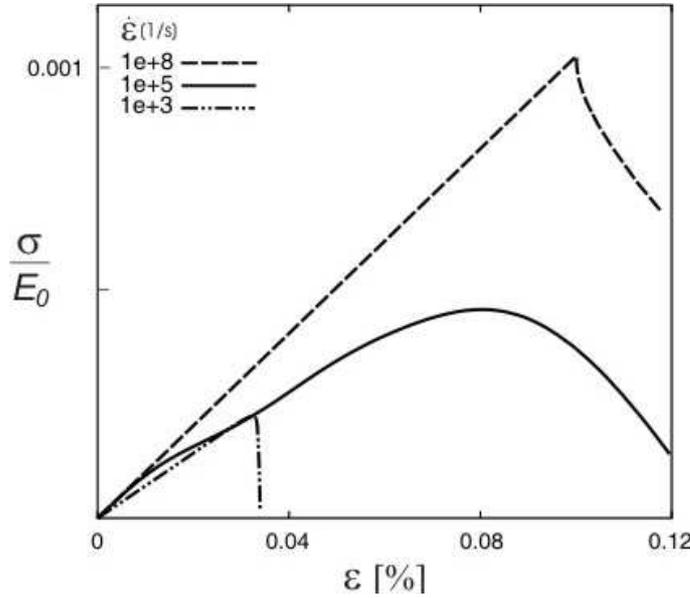
Figure 1: Three typical stress-strain curves for the tension test for geometrically and structurally disordered sample ($\alpha = 0.02$, $\beta = 0.5$).

disorder, $\alpha \approx 0$, possible for this model (Section 3), which results in the most extreme difference between the two slopes (Table 1).

The slopes of the dashed stress-strain curves, corresponding to $\dot{\varepsilon} = 1 \times 10^8\,s^{-1}$ and $\dot{\varepsilon} = 1 \times 10^3\,s^{-1}$, appear to be typical of the higher (from $3 \times 10^5\,s^{-1}$ to $1 \times 10^8\,s^{-1}$) and the moderate loading rates (from $1\,s^{-1}$ to $1 \times 10^4\,s^{-1}$), respectively. The solid stress-strain curve at $\dot{\varepsilon} = 1 \times 10^5\,s^{-1}$, with the characteristic "hump", marks the transition between the two groups.

A closer examination reveals that the described behavior is not sensitive to the choice of the computational time step, the sample aspect ratio, or the specifics of either the loading procedure or details of the constitutive

---

[1]The stress is the sample-average quantity obtained in the usual molecular dynamics manner [11].

Table 1: Ratio of the short-time and long-time moduli of elasticity for various combinations of geometrical and structural disorder.

$E_{st}^{(\varepsilon)} \big/ E_{lt}^{(\varepsilon)}$		α			
		0.02	0.2	0.5	1
β	0.2	1.59	1.45	1.30	1.22
	0.5	1.35	1.25	1.13	1.06
	1	1.27	1.17	1.06	1.00

law. Needless to say, the behavior is also insensitive to the particular realizations of the geometrical and structural disorder (reflected by the choice of the pseudorandom-number-generator seed).[2]

2 Elastic properties of two-dimensional systems

The Hooke's law for a three-dimensional isotropic material can be written as

$$\varepsilon_{11} = \frac{1}{E} \left[\sigma_{11} - \upsilon \left(\sigma_{22} + \sigma_{33} \right) \right] \quad and \quad \varepsilon_{12} = \frac{1 + \upsilon}{E} \sigma_{12} \tag{1}$$

along with four other similar expressions. In Eq. (1) E and υ are the mechanical properties of the material, namely, the modulus of elasticity and the Poisson's ratio, respectively.

It is often convenient, when dealing with 2D problems, to write the stress-strain relationship in the similar form

$$\varepsilon_{11} = \frac{1}{E^{(2D)}} \left[\sigma_{11} - \upsilon^{(2D)} \sigma_{22} \right] \quad and \quad \varepsilon_{12} = \frac{1 + \upsilon^{(2D)}}{E^{(2D)}} \sigma_{12} \tag{2}$$

where coefficients $E^{(2D)}$ and $\upsilon^{(2D)}$ are, formally, 2D counterparts of the material properties E and υ. Obviously, $E^{(2D)}$ and $\upsilon^{(2D)}$ are nothing more then coefficients which are obtained by combining the actual material properties under the conditions of:

•the plane strain $(2D = \varepsilon : \quad \varepsilon_{33} = \varepsilon_{13} = \varepsilon_{23} = 0)$

$$E^{(\varepsilon)} = \frac{E}{1 - \upsilon^2} \tag{3}$$

---

[2]The identical initial elastic response is obtained by performing 30 statistical realizations with different seed numbers.

•the plane stress $(2D = \sigma : \quad \sigma_{33} = \sigma_{13} = \sigma_{23} = 0)$

$$E^{(\sigma)} = E \tag{4}$$

Specifically, for the plane-strain problem with the imposed constraint

$$\sigma_{22} = 0 \quad \Leftrightarrow \quad \varepsilon_{22} = -\frac{\upsilon}{1-\upsilon}\,\varepsilon_{11} \tag{5}$$

the slope of the $\sigma_{11} - \varepsilon_{11}$ curve is $E^{(\varepsilon)} = E/(1 - \upsilon^2)$.

The plane-strain stiffness components are sample-average quantities obtained in the usual molecular dynamics manner during simulations [11]. Hence, it is convenient to express the modulus of elasticity, E, in terms of the plane-strain stiffness components

$$E = \frac{C_{12}^{(\varepsilon)}\left(3\,C_{11}^{(\varepsilon)} - 4\,C_{12}^{(\varepsilon)}\right)}{C_{11}^{(\varepsilon)} - C_{12}^{(\varepsilon)}} \tag{6}$$

Eq.(6) follows from the stiffness coefficient matrix

$$\left[C_{ab}^{(\varepsilon)}\right] = \begin{bmatrix} C_{11}^{(\varepsilon)} & C_{12}^{(\varepsilon)} & C_{16}^{(\varepsilon)} \\ C_{21}^{(\varepsilon)} & C_{22}^{(\varepsilon)} & C_{26}^{(\varepsilon)} \\ C_{61}^{(\varepsilon)} & C_{62}^{(\varepsilon)} & C_{66}^{(\varepsilon)} \end{bmatrix} = \frac{E}{(1+\upsilon)\,(1-2\upsilon)} \begin{bmatrix} 1-\upsilon & \upsilon & 0 \\ \upsilon & 1-\upsilon & 0 \\ 0 & 0 & (1-2\upsilon)/2 \end{bmatrix} \tag{7}$$

corresponding to the apparent plane-strain constitutive equations [8]. (Notice the compacted notation in Eqs. (6) and (7): $11 \rightarrow 1$, $22 \rightarrow 2$, and $12 \rightarrow 6$.)

Also, notice that the isotropy condition $C_{66}^{(\varepsilon)} = \left(C_{11}^{(\varepsilon)} - C_{12}^{(\varepsilon)}\right)\big/2$ and the symmetry condition $C_{12}^{(\varepsilon)} = C_{66}^{(\varepsilon)}$ imply that

$$C_{12}^{(\varepsilon)} = \frac{C_{11}^{(\varepsilon)}}{3} \tag{8}$$

Since Eq.(8) is satisfied by 2D lattices with the central-force interaction, Eq.(6) is reduced to

$$E = \frac{5}{6}\,C_{11}^{(\varepsilon)} \tag{9}$$

while from Eqs. (3) and (9) it follows that

$$E^{(\varepsilon)} = \frac{8}{9}\,C_{11}^{(\varepsilon)} \tag{10}$$

Finally, keeping in mind the relationship between the plane-strain modulus of elasticity and the link stiffness of the triangular lattice with the nearest-neighbor central-force interaction, $E^{(\varepsilon)} = 2\,k\big/\sqrt{3}$, [7], it is obvious, based on Eqs. (3) and (9) that

$$E = \frac{5\sqrt{3}}{8}\,k \qquad (11)$$

Eq.(11) provides an important connection between the modulus of elasticity and the link stiffness (or the average link stiffness, $\bar{k}$, in the case of the structurally disordered lattice, $\beta < 1$; see Section 3) of the said lattice.

3   Details of the simulation

The simulations of the dynamic uniaxial tension test presented herein are performed under the homogeneous loading conditions, which implies that an initial velocity field is imposed on the lattice at $t = 0$ [5].[3] The initial velocity $\pm\dot\varepsilon\,L/2$ at the top (+) and bottom (−) surface of the specimen, is defined in terms of the prescribed strain rate, $\dot\varepsilon = \dot{L}\big/L$, where L is the length of the sample, and dot is used to denote differentiation with respect to time. A homogeneous velocity gradient is imposed to all other particles in the loading direction according to the linear form $\dot{y} = \dot\varepsilon\,y$. Subsequently, at $t > 0$, only velocities of the particles located at the top and bottom boundaries ($\pm L/2$) are controlled, while the motion of the other particles is governed by equation of motion. The lateral inertia is overcome in a similar manner by applying a velocity $\dot{x} = v_0\,\dot\varepsilon\,x$ to all lattice particles at $t = 0$, where v_0 is the Poisson's ratio. As a direct consequence of the initial velocity field applied perpendicular to the loading ($y-$) direction, the stress in the lateral ($x-$) direction is approximately zero regardless of the strain rate of the external load applied in the longitudinal direction (i.e., $\sigma_x = \sigma_2 \approx 0 \quad \forall\dot\varepsilon$).

The lattice link properties are a combination of a linear force-elongation relation in tension (the Hookean potential), and a nonlinear force-deformation relation in compression (inspired by the Born-Meyer potential [7]).

The lattice morphology is defined by the coordination number z and the link length λ. The average distance between two neighboring particles ($\bar\lambda$)

---

[3]Although the inhomogeneous tension simulation is a natural simulation setup in a sense that it mimics the corresponding laboratory experiment, it is, unfortunately, limited to moderate strain rates; at high strain rates the top- and bottom-boundary particles, to which the prescribed displacement is applied, separate from the rest of the lattice since the fracture criterion is defined in terms of a relatively small critical link extension and the loading power is extremely high. This unavoidable shortcoming limits application of the inhomogeneous loading models.

is the model resolution length (l_c). In the pristine state all lattices used in this study are topologically ordered by selecting $z = 6$ for all bulk-particles. The lattice is geometrically disordered since the equilibrium distances between particles (initial link lengths $\equiv \lambda_0$) are sampled from the normal distribution within the range $\left[\alpha\bar{\lambda} \leqslant \lambda_0 \leqslant (2 - \alpha)\,\bar{\lambda}\right]$. The geometrical-order parameter α, $(0 \leqslant \alpha \leqslant 1)$, is the model parameter that defines bandwidth of the geometrical disorder of the material (Fig. 3). The lattice is also structurally (chemically)
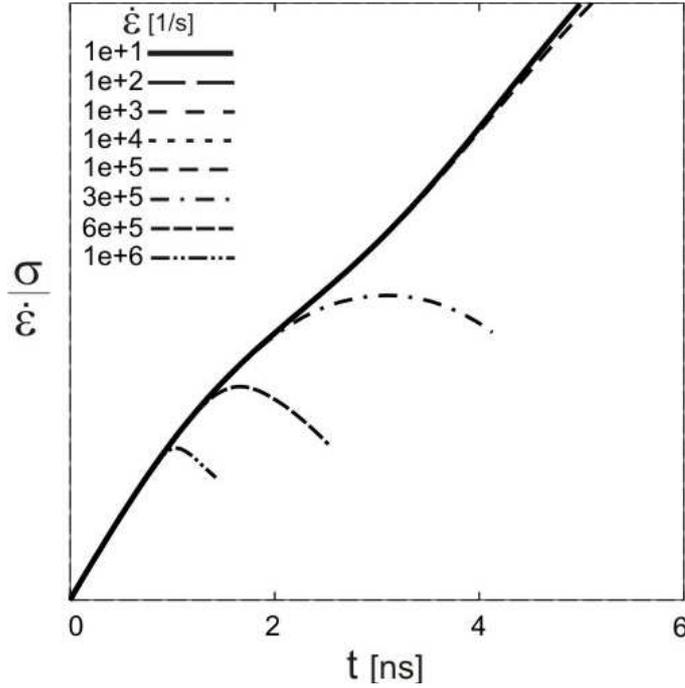
Figure 2: Time history of the stress normalized by the corresponding strain rate for the tension test at eight different loading rates.

disordered. The link stiffnesses are uniformly distributed within the range $\left[\beta\bar{k} \leqslant k \leqslant (2 - \beta)\,\bar{k}\right]$, where β, $(0 \leqslant \beta \leqslant 1)$, is the structural-order parameter defining the stiffness distribution.

The uniaxial tension simulations are performed on the 192×227 triangular lattice. The lattice size is chosen based on a size-effect analysis to ensure the size-independency of the results.

The reduced-units geometric and structural parameters of the lattice are: the mean link stiffness $\bar{k} = 50$, the mean equilibrium distance between particle sites $\bar{\lambda} = l_c = 1$, while the geometrical-order parameter, α, and the structural-order parameter, β, are variables subject to this analysis.
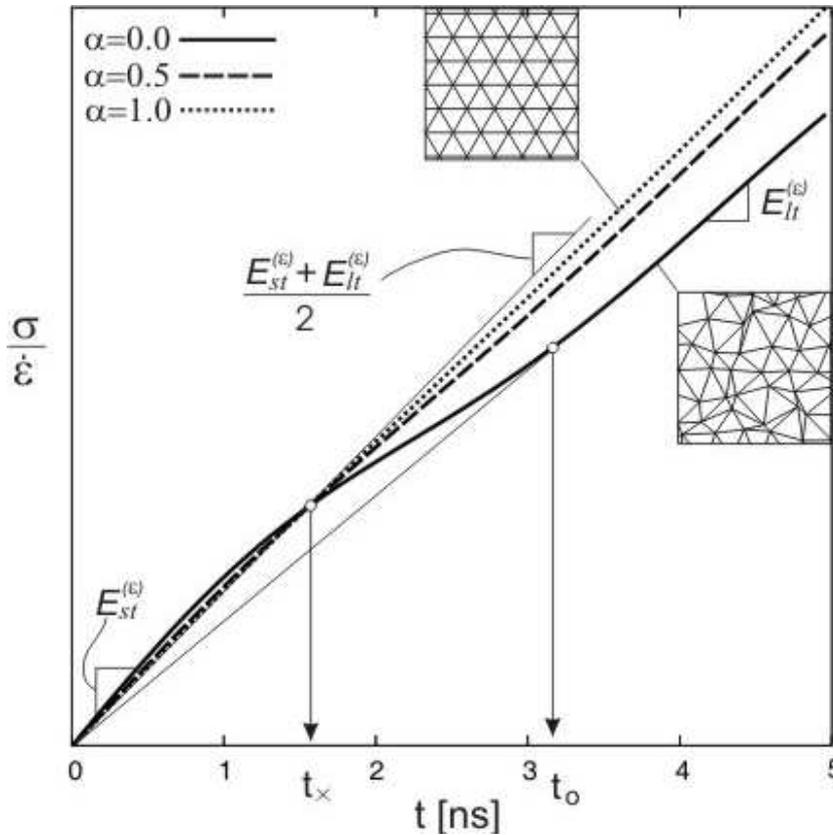
Figure 3: Time history of the stress normalized by the corresponding strain rate for the homogeneous tension test at three different levels of geometrical disorder.

4 Results

The history of the stress divided by the corresponding loading rate for eight different strain rates (the four lowest loading rates are overlapped by the solid line) is presented in Fig. 2. It is evident that the two characteristic slopes are the short-time and long-time moduli, observed previously in Fig. 1, presented herein in a more convenient graph. The solid curve is common for all loading rates that remain elastic for the given graph limits; the departures from that curve mark onsets of the inelastic deformation that is characterized by damage nucleation and, depending on the loading rate, different levels of microcrack cooperative phenomena. It may be inferred based on Fig. 2 that the characteristic transition from the short-time modulus to the long-time modulus, observed in Fig. 1, is common for *all* loading rates – the only difference is that for the more rapid loading rates the specimen fails before the transition

time is reached. This is consistent with the observation of the stiffness tensor evolution: namely, the stiffness tensor components (for the same α) remain unchanged as long as the deformation is elastic. Another observation is that the ratio of the short-time and long-time moduli depends strongly on the geometrical and structural disorder, defined, respectively, by parameters α and β (see also Fig. 3).[4] This qualitative observation is quantified in Table 1 with three significant digits.

Finally, two characteristic times, describing the $E_{st}^{(\varepsilon)} \rightarrow E_{lt}^{(\varepsilon)}$ transition, are depicted in Fig. 3. The crossover time, defined by equal normalized stress $(\sigma/\dot{\varepsilon})$ regardless of the geometrical order parameter, is designated by t_x. The transition time at which the $E_{st} \rightarrow E_{lt}$ transition is completed is designated by $t_\bigcirc$. The latter characteristic time is independent of the geometrical disorder level (i.e., α-independent). Fortuitously or not, the simulation data suggest that

$$t_o \approx 2 \ \frac{l_c}{C_0} \approx 2 \ t_\times \tag{12}$$

where C_0 is velocity of the elastic longitudinal wave propagation.

The stiffness components and apparent plane-strain elastic moduli for various combinations of geometrical and structural disorder are presented in Tables 2 and 3.

Table 2: Stiffness components and elastic moduli for structurally ideal ($\beta = 1$) and geometrically disordered triangular lattice.

α	0.02	0.4	0.6	1.0
$C_{11} = C_{22} = 3C_{12}$	75.0	68.7	66.6	64.8
$E_{st}^{(\varepsilon)}$	65.3	60.5	58.8	57.6
$E_{lt}^{(\varepsilon)}$	49.6	54.8	56.3	57.6
$\left(E_{st}^{(\varepsilon)} + E_{lt}^{(\varepsilon)} \right) \big/ 2$	57.5	57.7	57.6	57.6

Note: For the triangular lattice with the first-neighbor central interactions $E^{(\varepsilon)} = 2\,\bar{k} \big/ \sqrt{3} = 57.7$ [7] and $E^{(\varepsilon)} = 8\,C_{11}^{(\varepsilon)} \big/ 9$

It is obvious from these results that the triangular lattice is equivalent to the elastic solid under the plane strain conditions only in absence of disorder ($\alpha = 1$, $\beta = 1$). As long as the disorder is moderate ($\alpha \geqslant 0.5$, $\beta \geqslant 0.5$) the discrepancy between the lattice and solid $E^{(\varepsilon)}$ is within 10% for any combination of α and β (Tables 1 through 3). It is interesting to note that in the

---

[4]The emphasis is on the effect of disorder because of the homogeneous simulation setup that, as previously mentioned, cancels out the lateral inertia effects. In absence of this numerical artifice, at the onset of high strain rate loading $\varepsilon_2 \ (t = 0^+) \approx 0$ and $E^{(\varepsilon)} \approx C_{11}^{(\varepsilon)}$.

Table 3: Stiffness components and elastic moduli for geometrically ideal ($\alpha = 1$; all grains are perfect hexagons) and structurally disordered triangular lattice under the homogeneous tension.

β	0.0	0.5	0.8	1.0
$C_{11} = C_{22} = 3C_{12}$	64.8	64.8	64.8	64.8
$E_{st}^{(\varepsilon)}$	56.8	57.3	57.5	57.6
$E_{lt}^{(\varepsilon)}$	39.0	54.1	57.0	57.6
$\left(E_{st}^{(\varepsilon)} + E_{lt}^{(\varepsilon)}\right)/2$	47.9	55.7	57.3	57.6

case of structurally ideal lattice ($\beta = 1$) the average value of the short-term and long-term lattice moduli remains practically unchanged and corresponds to the analytically obtained value $E^{(\varepsilon)} = 2\bar{k}/\sqrt{3}$ [7].[5]

5 Conclusion

Although the triangular lattice earned its place in modeling of the elastic behavior, damage evolution, and fracture behavior of inhomogeneous or multiphase systems some issues concerning limits of their applicability and drawbacks had been recognized in the past (e.g., [2, 3, 7]). It is important to indicate that the lattice behavior is rigorously equivalent to the behavior of a solid only as long as the lattice is ideal (that is, in absence of disorder). As soon as the disorder is introduced, the behavior of a solid could only be approximated by the behavior of the 2D systems, with the degree of accuracy that decreases with the level of disorder "quenched" within the lattice. It is demonstrated in this study that for a strongly disordered lattice the modulus of elasticity disagrees noticeably from its solid body counterpart.

References

[1] A. Brara, F. Camborde, J.R. Klepaczko, C. Mariotti, Experimental and numerical study of concrete at high strain rates in tension, Mech. Mater., 33, (2001), 33-45.

---

[5]According to Fig. 3, this slope $E^{(\varepsilon)} = 2\bar{k}/\sqrt{3} \approx \left(E_{st}^{(\varepsilon)} + E_{lt}^{(\varepsilon)}\right)/2$ is defined by the crossover time t_x.

[2] W.A. Curtin and H. Scher, Brittle fracture in disordered materials: a spring network model, J. Mater. Res., 5, (1990), 535-553.

[3] A. Jagota and S.J. Bennison, Spring-Network and Finite-Element Models for Elasticity and Fracture, In Proceedings of a workshop on breakdown and non-linearity in soft condensed matter, eds. K.K. Bardhan, B.K. Chakrabarti, A. Hansen, Springer-Verlag Lecture Notes in Physics, Berlin, (1994), 186-201.

[4] D. Krajcinovic, Damage Mechanics, North-Holland, Amsterdam, 1996.

[5] S. Mastilovic and D. Krajcinovic, Statistical Models of Brittle Deformation, Part Two: Computer Simulations, Int. J. Plast., 15, (1999), 427-456.

[6] S. Mastilovic, A. Rinaldi, D. Krajcinovic, Ordering effect of kinetic energy on dynamic deformation of brittle solids, Mech. Mater., 40, (2008), 407-417.

[7] L. Monette, M.P. Anderson, Elastic and fracture properties of the two-dimensional triangular and square lattices, Modelling Simul. Mater. Sci. Eng., 2, (1994), 53-66.

[8] S. Nemat-Nasser, M. Hori, Micromechanics: Overall Properties of Heterogeneous Materials, North-Holland, Amsterdam, 1994.

[9] A. Rinaldi, D. Krajcinovic, P. Peralta, Y. Lai, Lattice models of polycrystalline microstructures: A quantitative approach, Mech. Mater., 40, (2008), 17-36.

[10] M. Sahimi, Heterogeneous material II. Springer. New York, 2000.

[11] V. Vitek, Pair potentials in atomistic computer simulations, In Interatomic Potentials for Atomistic Simulations, MRS Bulletin, 21 (2), ed. A.F. Voter, (1996).

O elastičnom odzivu neuredjene trougaone mreže tokom dinamičkog opterećenja

Ovo ispitivanje se bavi opažanjem koje se odnosi na inicijalni elastični odziv trougaone, geometriski i strukturno neuredjene, mreže tokom opterećenja u opsegu od srednjih do visokih brzina deformisanja. Radi se o tranziciji od kratkoročnog na dugoročni moduo elastičnosti, koja nije praćena odgovarajućom promenom tenzora čvrstoće. Pokazano je da je razlika izmedju dva modula, u slučaju ovde korišćenih simulacija homogenih dvoosnih testova na zatezanje, posledica geometrijske i strukturne neuredjenosti mreže. Ispitivanje je izvršeno na trougaonoj mreži sa centralnim interakcijama sa prvim susedima, pod praktično identičnim ravanskim uslovima u opsegu od osam dekada brzina deformisanja.